Quadrature Control-Bounded ADCs

Hampus Malmberg[1], Fredrik Feyling[2], and Jose M de la Rosa[3]
Dept. of Information Technology & Electrical Engineering, ETH Zürich, Zürich, Switzerland[1]
Dept. of Electronic Systems, Norwegian University of Science and Technology, Trondheim, Norway[2]
Institute of Microelectronics of Seville, IMSE-CNM (CSIC/University of Seville), Seville, Spain[2]

***Abstract*—In this paper, the design flexibility of the control-bounded analog-to-digital converter principle is demonstrated by considering band-pass analog-to-digital conversion. We show how a low-pass control-bounded analog-to-digital converter can be translated into a band-pass version where the guaranteed stability, converter bandwidth, and signal-to-noise ratio are preserved while the center frequency for conversion can be positioned freely. The proposed converter is validated with behavioral simulations for a variety of filter orders, notch-filter frequencies, and oversampling ratios. Finally, robustness against component variations is demonstrated by Monte Carlo simulations.**

***Index Terms*—Analog-to-digital converters, control-bounded, quadrature and band-pass sigma-delta modulation.**

I. Introduction

Band-pass sigma-delta modulators (BP-$\Sigma\Delta$Ms) allow digitizing non base-band signals; essentially expediting the role and position of analog-to-digital (A/D) conversion in the receive structure of a wireless receivers. A mainly digital wireless receive path is lucrative as digital signal processing offers better technology scaling and programmability towards a software-define-radio (SDR) platform [1]–[3]. Digitizing radio frequency (RF) signals typically utilize sampling frequencies in the GHz range. Hence, state-of-the-art BP-$\Sigma\Delta$Ms are mostly implemented using continuous-time (CT) circuits as they offer inherent anti-aliasing filtering and are potentially faster and more power efficient than their discrete-time (DT) counterparts. However, in the majority of cases, RF BP-$\Sigma\Delta$Ms have a fixed ratio between the center or *notch* frequency, f_n, and the sampling frequency f_s (typically $f_n = f_s/4$). A fixed f_s/f_n ratio results in two main limitations: firstly, for wireless standards operating around 2.5-5GHz, prohibitive values of f_s, in the order of tens of GHz, are typically required. Secondly, a widely programmable phase-locked loop (PLL) is required for tuning f_n while keeping the f_s/f_n ratio fixed. These limitations have prompted the interest for reconfigurable BP-$\Sigma\Delta$Ms with tunable notch frequency [4]. However, reported solutions are limited in practice by the increased (analog) circuit complexity and risk of potential instability of the loop filter – compromised by the tuning range of f_n [4].

Control-bounded A/D conversion offers an alternative solution to the problem of digitizing RF signals. The quadrature control-bounded analog-to-digital converter (Q-CBADC) is a highly modular architecture with a tunable f_n and comes with a stability guarantee. The Q-CBADC follows from extending two low-pass control-bounded analog-to-digital converters (CBADCs) into a single oscillating structure. Conveniently, the Q-CBADC's signal-to-noise ratio (SNR) and bandwidth (BW) specification follows from its two low-pass CBADCs building blocks. Like quadrature sigma-delta modulators (Q-$\Sigma\Delta$Ms) [6], the Q-CBADCs is a quadrature analog-to-digital converter (ADC) resulting in the same number of integrating stages per signal as its low-pass building block.

II. The Leapfrog Analog Frontend

The fundamental principle of a CBADC is that the interaction between analog amplification and digital control loops amounts to an implicit A/D conversion. In the low-pass leapfrog (LF) CBADC [7], the amplification is provided by the LF analog system (AS), see the dashed boxes in Fig. 1. Specifically, the input signal $u(t)$ is amplified through a chain-of-integrators structure where the output of the ℓth integrator is referred to as the ℓth state $x_\ell(t)$ of the AS. The AS is stabilized by a digital feedback loop, referred to as the digital control (DC). The DC consist of a single bit quantizer, clocked at $f_s \triangleq 1/T$, generating the discrete-time control signals $s_\ell[k]$, which are mapped to the continuous-time domain through a digital-to-analog converter (DAC) with an impulse response $\theta(t)$. The continuous-time control signal $s_\ell(t) = \sum_k s_\ell[k]\theta_\ell(t-kT)$ is added to the input of the ℓth integrator, and as a result, $x_\ell(t)$ remain bounded.

The CBADC's final output follows from the control signals as

$$\hat{u}[k] \triangleq \sum_{\ell=1}^{N} (h_\ell * s_\ell)[k]. \tag{1}$$

where the finite impulse response (FIR) filter coefficient's $h_1[.], \dots, h_\ell[.]$, in (1), depend on the parametrization of the analog frontend (AF), i.e., the combined AS and DC. In case of component variations, a significant error follows from not updating the filter coefficients accordingly [8]. The filter coefficients can analytically be calculated as in [9] or alternatively by calibration as in [10].

The AS of a CBADC is conveniently described using state-space equations. We define an Nth order LF AS, by the system of differential equations

$$\dot{\boldsymbol{x}}(t) = \boldsymbol{A}_{\mathrm{LF}}\boldsymbol{x}(t) + \boldsymbol{B}_{\mathrm{LF}}u(t) + \boldsymbol{s}(t) \tag{2}$$

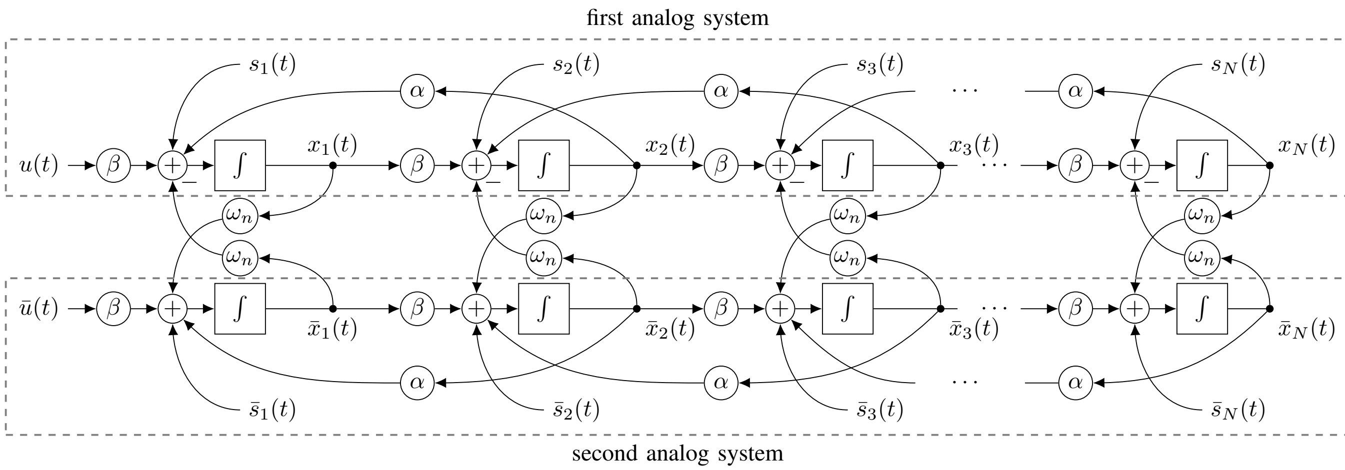

Fig. 1. The quadrature Leapfrog analog system which is is the combination of two Leapfrog structures, as in Section II, connected by the ω_n paths. The system is stabilized using the quadrature local digital control in Fig. 2.

for the analog state vector $\boldsymbol{x}(t) \triangleq \left(x_1(t), \ldots, x_N(t)\right)^\mathsf{T}$, the control signal contribution vector $\boldsymbol{s}(t) \triangleq \left(s_1(t), \ldots, s_N(t)\right)^\mathsf{T}$,

$$\boldsymbol{A}_{\text{LF}} \triangleq \begin{pmatrix} 0 & \alpha & & \\ \beta & 0 & \ddots & \\ & \ddots & \ddots & \alpha \\ & & \beta & 0 \end{pmatrix} \in \mathbb{R}^{N \times N}, \tag{3}$$

and $\boldsymbol{B}_{\text{LF}} \triangleq \left(\beta, 0, \ldots, 0\right)^\mathsf{T} \in \mathbb{R}^N$.

The LF's simplistic and modular structure enables design equations where for a given N, $\omega_\mathcal{B}$, and $\text{OSR} \triangleq \frac{\pi f_s}{\omega_\mathcal{B}}$,

$$\text{SNR} \propto (\text{OSR})^{2N} \tag{4}$$

and system stability follows from

$$|\beta| = \frac{\omega_\mathcal{B} \cdot \text{OSR}}{2\pi} \tag{5}$$

$$\beta = -\kappa = -\frac{\omega_\mathcal{B}^2}{4\alpha} \tag{6}$$

where $\omega_\mathcal{B}$ [rad/s] is the signal bandwidth. It was shown in [8] that the nominal performance of a LF ADC is similar to that of a heuristically optimized continuous-time sigma-delta modulator (CT-$\Sigma\Delta$M) with the same loop filter order N, fixed OSR, and the same number of comparators.

III. Quadrature Analog Frontends

Two low-pass CBADC, as in Section II, can be turned into a quadrature CBADC by two modifications: firstly, interconnecting the two AS such that they oscillate at the desired notch frequency $\omega_n = 2\pi f_n$, as shown in Fig. 1. Secondly, the resulting AS can be stabilized by a local quadrature DC as given in Fig. 2. This general principle applies to any low-pass CBADC AF. In this paper, only the LF AS will be transformed into its quadrature version.

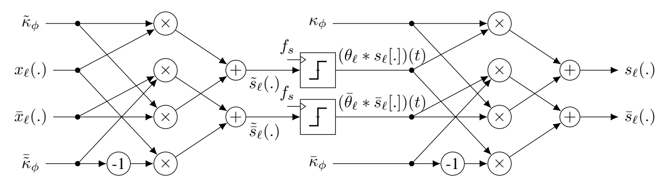

Fig. 2. The ℓth local quadrature DC, connecting $\boldsymbol{x}_\ell(t) = (x_\ell(t), (\bar{x}_\ell(t))$ with $\boldsymbol{s}_\ell = (s_\ell(.), \bar{s}_\ell(.))$ in Fig. 1. The output of the two comparators are considered continuous-time quantities $((\theta_\ell * s_\ell[.])(t), (\bar{\theta}_\ell * \bar{s}_\ell[.])(t))$, where $(\theta_\ell(.), \bar{\theta}_\ell(.))$ are the comparators' impulse responses and $(s[.], \bar{s}[.])$ are the discrete-time control decisions used in (1).

A. Quadrature Analog System

For a quadrature AS to oscillate at a desired angular frequency ω_n, two Nth order ASs are stacked in parallel and interconnected as

$$\begin{pmatrix} \dot{\boldsymbol{x}}(t) \\ \dot{\bar{\boldsymbol{x}}}(t) \end{pmatrix} = \boldsymbol{A} \begin{pmatrix} \boldsymbol{x}(t) \\ \bar{\boldsymbol{x}}(t) \end{pmatrix} + \boldsymbol{B} \begin{pmatrix} u(t) \\ \bar{u}(t) \end{pmatrix} + \begin{pmatrix} \boldsymbol{s}(t) \\ \bar{\boldsymbol{s}}(t) \end{pmatrix} \tag{7}$$

$$\boldsymbol{A} \triangleq \begin{pmatrix} \boldsymbol{A}_{\text{LF}} & -\omega_n \boldsymbol{I}_N \\ \omega_n \boldsymbol{I}_N & \boldsymbol{A}_{\text{LF}} \end{pmatrix} \in \mathbb{R}^{2N \times 2N} \tag{8}$$

$$\boldsymbol{B} \triangleq \begin{pmatrix} \boldsymbol{B}_{\text{LF}} & \boldsymbol{0}_N \\ \boldsymbol{0}_N & \boldsymbol{B}_{\text{LF}} \end{pmatrix} \in \mathbb{R}^{2N \times 2} \tag{9}$$

where $\boldsymbol{A}_{\text{LF}}$ and $\boldsymbol{B}_{\text{LF}}$ refers to the system description in Section II and $\boldsymbol{x}(t)$, $\bar{\boldsymbol{x}}(t)$, and $\boldsymbol{s}(t)$, $\bar{\boldsymbol{s}}(t)$ are the in-phase and quadrature part of the state vector and control signal vector, respectively. Equations (7)-(9), applied to the LF AS from Section II, are visualized in Fig. 1.

B. Local Quadrature Digital Control

The quadrature AS can be stabilized by local quadrature DCs as shown in Fig. 2. Here each quadrature state pair $\boldsymbol{x}_\ell(t) \triangleq \left(x_\ell(t), \bar{x}_\ell(t)\right)^\mathsf{T}$ are turned into a control observation

$$\tilde{\boldsymbol{s}}_\ell(t) \triangleq \begin{pmatrix} \tilde{s}_\ell(t) \\ \bar{\tilde{s}}_\ell(t) \end{pmatrix} = \begin{pmatrix} \tilde{\kappa}_\phi & -\bar{\tilde{\kappa}}_\phi \\ \bar{\tilde{\kappa}}_\phi & \tilde{\kappa}_\phi \end{pmatrix} \boldsymbol{x}_\ell(t) \tag{10}$$

which is sampled and quantized into the quadrature discrete-time control signal pair $\boldsymbol{s}_\ell[k] \triangleq \left(s_\ell[k], \bar{s}_\ell[k]\right)^\mathsf{T}$. For a non-return to zero DAC the ℓth quadrature control contribution pair follows as

$$\boldsymbol{s}_\ell(t) \triangleq \begin{pmatrix} s_\ell(t) \\ \bar{s}_\ell(t) \end{pmatrix} = \begin{pmatrix} \kappa_\phi & -\bar{\kappa}_\phi \\ \bar{\kappa}_\phi & \kappa_\phi \end{pmatrix} \boldsymbol{s}_\ell[k] \tag{11}$$

for $t \in ((k-1)T + \tau_{\text{DC}}, kT + \tau_{\text{DC}}]$ where $\tau_{\text{DC}} > 0$ is the time delay associated with the quantizer.

To determine the required values of κ_ϕ, $\bar{\kappa}_\phi$, $\tilde{\kappa}_\phi$, and $\bar{\tilde{\kappa}}_\phi$ for stabilizing the system, we extend the approach in [7] for stabilizing a chain-of-integrators AS to the quadrature AS case. Specifically, $(\kappa_\phi, \bar{\kappa}_\phi, \tilde{\kappa}_\phi, \bar{\tilde{\kappa}}_\phi, T)$ are chosen such that, at the end of a control-period T, each quadrature state pair $\|\boldsymbol{x}_\ell(T)\|_2 < \epsilon$ for any quadrature input pair $\|\boldsymbol{x}_{\ell-1}(t)\|_2 < \epsilon$, and initial state $\|\boldsymbol{x}_\ell(0)\|_2 < \epsilon$, where $t \in [0, T)$ and $\epsilon > 0$. It follows that if such a parametrization exists, the system as a whole will be inherently stable by a recursive argument given the first quadrature input pair $\|\boldsymbol{x}_0(t)\|_2 \triangleq \|\left(u(t), \bar{u}(t)\right)\|_2 < \epsilon$. The proposed approach reduces to upholding the following conditions:

1) Considering the largest possible quadrature input and control signal separately, each contribution to the state norm $\|\boldsymbol{x}_\ell(kT)\|_2$ must be equal at the end of an arbitrary control period k.
2) The DC is self stable, i.e., for any initial quadrature state vector $\|\boldsymbol{x}_\ell((k-1)T)\|_2 < \epsilon$, $\boldsymbol{x}_{\ell-1}(t) \overset{!}{=} \left(0, 0\right)^\mathsf{T}$, and $t \in [(k-1)T, kT)$, the quadrature control contribution preserves $\|\boldsymbol{x}_\ell(kT)\|_2 < \epsilon$.
3) For $\boldsymbol{x}_\ell(0) = \left(0, 0\right)^\mathsf{T}$, any superposition of quadrature input and control signal must not make $\|\boldsymbol{x}_\ell(T)\|_2 > \epsilon$.

Using the parametrization in Fig. 1 and Fig. 2, these general conditions can be reduced to design equations for the involved parameter values. The steps involved include analytical solutions to systems of differential equations, properties of norms and rotation matrices. Given the space limitation, only the resulting expressions will be presented. Simulation results will be shown in Section IV to illustrate and validate the relevance of these mathematical expressions.

1) Matched Signal Strengths: The first condition can be satisfied by equating the normed quadrature state vector solution for the largest bounded contribution from the input signal and the control signal independently. The resulting expression reduces to the condition

$$\sqrt{\kappa_\phi^2 + \bar{\kappa}_\phi^2} \overset{!}{=} \frac{\beta T \omega_n}{2 \sin\left(\frac{\omega_n T}{2}\right)}. \tag{12}$$

2) Self Stability: Follows if the DC can anticipate the trajectory of an initial quadrature state vector $\boldsymbol{x}_\ell((k-1)T)$, and counteract the state norm growth by some control decision $\boldsymbol{s}_\ell[k-1]$ at the end of control period k. Solving the involved state trajectories and aligning the involved rotations results in the two conditions

$$\sqrt{\tilde{\kappa}_\phi^2 + \bar{\tilde{\kappa}}_\phi^2} \overset{!}{=} \frac{\omega_n}{2\sqrt{\kappa_\phi^2 + \bar{\kappa}_\phi^2} \sin\left(\frac{\omega_n T}{2}\right)} \tag{13}$$

$$\arctan\left(\frac{\bar{\tilde{\kappa}}_\phi}{\tilde{\kappa}_\phi}\right) \overset{!}{=} \omega_n \left(\frac{T}{2} + \tau_{\text{DC}}\right) - \phi_\kappa + \pi, \tag{14}$$

where $\phi_\kappa = \arctan\left(\bar{\kappa}_\phi / \kappa_\phi\right)$. By combining (12), (13), and (14) follows

$$\kappa_\phi = \frac{\beta T \omega_n}{2 \sin\left(\frac{\omega_n T}{2}\right)} \cos\left(\phi_\kappa\right) \tag{15}$$

$$\bar{\kappa}_\phi = \frac{\beta T \omega_n}{2 \sin\left(\frac{\omega_n T}{2}\right)} \sin\left(\phi_\kappa\right) \tag{16}$$

$$\tilde{\kappa}_\phi = -\frac{1}{\beta T} \cos\left(\omega_n \left(\frac{T}{2} + \tau_{\text{DC}}\right) - \phi_\kappa\right) \tag{17}$$

$$\bar{\tilde{\kappa}}_\phi = -\frac{1}{\beta T} \sin\left(\omega_n \left(\frac{T}{2} + \tau_{\text{DC}}\right) - \phi_\kappa\right) \tag{18}$$

where $\phi_\kappa \in [0, 2\pi)$ is a free parameter that may be chosen to ensure practical values.

3) Worst-Case Superposition: The third condition follows, as in the case of chain-of-integrators [7], by

$$2\beta T \leq 1. \tag{19}$$

In summary, the stability of a quadrature CBADC analog frontend, as in (7)-(9), can be ensured for $(\kappa_\phi, \bar{\kappa}_\phi, \tilde{\kappa}_\phi, \bar{\tilde{\kappa}}_\phi, T)$ as in (15)-(19). Fig. 3 illustrates an example of how these variables vary as a function of ω_n for $2\beta T = 1$ and $\phi_\kappa = 0$.

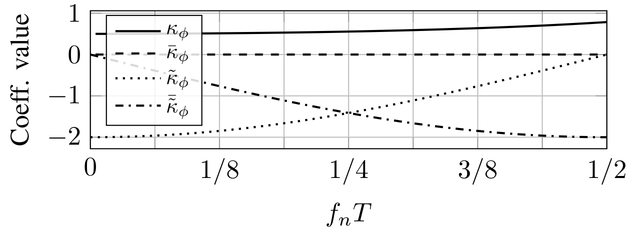

Fig. 3. The coefficients in (15)-(18) as a function of $\omega_n = 2\pi f_n$ where $2\beta T = 1$, $\phi_\kappa = 0$, and $\tau_{DC} = 0$.

C. Circuit Implementation Example

To demonstrate that (7)-(11) can be implemented using conventional circuit techniques, Fig. 4 shows a single-ended op-amp implementation of a single quadrature stage from Fig. 1, with a local quadrature control as in Fig. 2. The resistive and capacitive values follows as $R_\alpha C = \alpha^{-1}$, $R_\beta C = \beta^{-1}$, $R_\kappa C = \kappa^{-1}$, $R_{\bar{\kappa}} C = \bar{\kappa}^{-1}$, and $R_{\omega_n} C = \omega_n^{-1}$ for the time constants and $\tilde{\kappa} = \frac{R_{\tilde{\kappa}_I}}{R_{\bar{\kappa}_I} - R_{\tilde{\kappa}_I}} = \frac{R_{\tilde{\kappa}_Q}}{R_{\tilde{\kappa}_Q} + R_{\bar{\kappa}_Q}}$ and $\bar{\tilde{\kappa}} = \frac{R_{\bar{\tilde{\kappa}}_I}}{R_{\tilde{\kappa}_I} - R_{\bar{\tilde{\kappa}}_I}} = \frac{R_{\bar{\tilde{\kappa}}_Q}}{R_{\tilde{\kappa}_Q} + R_{\bar{\tilde{\kappa}}_Q}}$ where $R_{\tilde{\kappa}_I} \geq R_{\bar{\tilde{\kappa}}_I}$. The presented circuit topology, does have significant implementation challenges, in particular the voltage dividers involving $(R_{\tilde{\kappa}_I}, R_{\bar{\tilde{\kappa}}_I}, R_{\tilde{\kappa}_Q}, R_{\bar{\tilde{\kappa}}_Q})$ could beneficially be replaced by multi-input comparators and the negative resistors could be

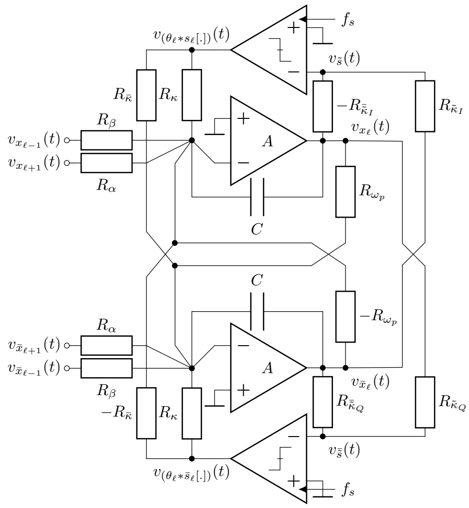

Fig. 4. A single-ended op-amp implementation of a single quadrature stage from Fig. 1 together with a local quadrature control as in Fig. 2.

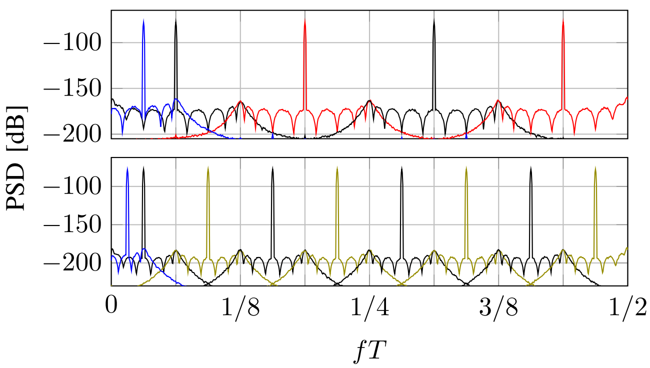

Fig. 5. PSD for different notch frequencies. The black, red, and yellow lines correspond to PSDs of (1) from Q-CBADCs designed for $\mathrm{OSR}/N = (4/8, 8/6)$ (top,bottom) and positioned at different notch filter frequencies f_n. Similarly, the blue lines are the PSDs of a corresponding low-pass CBADC building block.

managed in a differential setup. However, the purpose of Fig. 4 is to demonstrate that quadrature CBADC reduces to structures related to CT-$\Sigma\Delta$M circuit implementations.

IV. Simulation Results

Behavioral simulations, for multiple system specifications, where done in Python using the cbadc toolbox [11]. Each simulation used a full-scale sinusoidal input signal with a frequency f_n, $\phi_\kappa = \pi/3$, and $\tau_{\mathrm{DC}} = 0$. Subsequently, the in-phase component $u(t)$, from Fig. 1, was estimated as in (1). The resulting PSD for $\mathrm{OSR}/N = (4/8, 8/6)$ and multiple notch frequencies f_n are shown in Fig. 5. Note that, in contrast to the output of a CT-$\Sigma\Delta$Ms, the CBADC's output, (1), implicitly suppresses out-of-band frequencies. The SNRs, measured directly on the PSD, are approximately 74 and 101 dB respectively which are both ± 1 dB of the corresponding low-pass LF system performance (shown in blue in Fig. 5).

An important limiting factor for both BP-$\Sigma\Delta$M and Q-$\Sigma\Delta$M

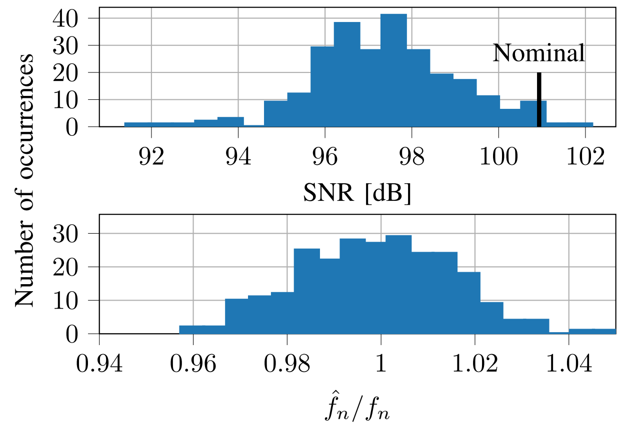

Fig. 6. Histograms showing variation in SNR (top) and estimated $\hat{f}_n$ normalized to nominal f_n (bottom) after 256 Monte Carlo simulations with up to $\pm 10\%$ variations in each individual $(\alpha, \beta, \omega_n, \kappa_\phi, \bar{\kappa}_\phi, \tilde{\kappa}_\phi, \tilde{\bar{\kappa}}_\phi)$ parameter.

is stability in the presence of component variations while targeting a wide tunable range. The proposed Q-CBADC's sensitivity to component variations was tested by 256 Monte Carlo simulations where each individual $(\alpha, \beta, \omega_n, \kappa_\phi, \bar{\kappa}_\phi, \tilde{\kappa}_\phi, \tilde{\bar{\kappa}}_\phi)$ value were drawn uniformly at random from within $\pm 10\%$ of their nominal values. For these simulations, the system was modeled using Verilog-A and simulated in Spectre with $\mathrm{OSR} = 8, N = 6$ and $f_n = 1/(4 f_s)$. The filter coefficients in (1) was calculated from the true system parameterization to avoid the additional filter mismatch error described in Section II.

Examining the resulting $\boldsymbol{x}(t), \bar{\boldsymbol{x}}(t)$ waveforms shows no sign of instabilities or increasing state amplitudes. Histograms of the resulting SNR performance and estimated notch frequencies $\hat{f}_n$ are given in Fig. 6. The results show SNRs and notch frequencies $\hat{f}_n$ in the ranges of $(-10, +1)$ dB, and $\pm 5\%$ from their respective nominal values. To the best of our understanding, the average reduction of $3 - 4$ dB SNR originates from the fact that the quadrature stages in Fig. 1 may loose amplification, in the transfer function from $(u(t), \bar{u}(t))$ to $(x_N(t), \bar{x}_N(t))$, by the combined effect of changes in bandwidth and non-aligning resonance frequencies per stage. This is different to the regular low-pass LF case [10], where the same simulation setup shows no significant change to average SNR when effectively only the bandwidth per stage vary. How to calibrate the digital estimator (DE), as was assumed in the above simulations, is further described in [10].

V. Conclusions

The Q-CBADC design principle extends any low-pass CBADCs into a quadrature version centered around a desired notch frequency without loss of SNR performance or stability margin. Nominal performance and tuning range is verified by behavioral simulations of different system orders and OSRs. Robustness is demonstrated by Monte Carlo simulations, with up to 10% component variations, resulting in a performance range of $(-10, +1)$ dB, relative nominal, SNR.

References

[1] A. Sayed *et al.*, "A 1.5-to-3.0GHz Tunable RF Sigma-Delta ADC With a Fixed Set of Coefficients and a Programmable Loop Delay," *IEEE Transactions on Circuits and Systems - II: Express Briefs*, vol. 67, pp. 1559–1563, September 2020.

[2] H. Ghaedrahmati, J. Zhou, and R. B. Staszewski, "A 38.6-fJ/Conv.-Step Inverter-Based Continuous-Time Bandpass $\Delta\Sigma$ ADC in 28 nm Using Asynchronous SAR Quantizer," in *IEEE Transactions on Circuits and Systems - II: Express Briefs*, vol. 68, pp. 3113–3117, September 2021.

[3] L. Jie *et al.*, "A 100MHz-BW 68dB-SNDR Tuning-Free Hybrid-Loop DSM with an Interleaved Bandpass Noise-Shaping SAR Quantizer," *IEEE ISSCC Digest of Technical Papers*, February 2021.

[4] G. Molina *et al.*, "LC-Based Bandpass Continuous-Time Sigma-Delta Modulators with Widely Tunable Notch Frequency," *IEEE Trans. on Circuits and Systems – I: Regular Papers*, pp. 1442–1455, May 2014.

[5] S. -B. Kim, T. D. Werth, S. Joeres, R. Wunderlich and S. Heinen, "Effect of Mismatched Loop Delay in Continuous-Time Complex Sigma-Delta Modulators," in *IEEE Transactions on Circuits and Systems - II: Express Briefs*, vol. 55, no. 10, pp. 996-1000, Oct. 2008.

[6] R. Schreier, G. C. Temes, "Bandpass and Quadrature Delta-Sigma Modulation," in *Understanding Delta-Sigma Data Converters*. New York, NY USA: Wiley, 2005, pp. 172-177.

[7] H. Malmberg, "Control-Bounded Converters," Ph.D. dissertation no. 27025, ETH Zürich, 2020

[8] F. Feyling, H. Malmberg, C. Wulff, H.-A Loeliger, and T. Ytterdal, "High-level comparison of control-bounded A/D converters and continuous-time sigma-delta modulators," in *Nordic Circuits and Systems Conference (NORCAS)*, Oslo, pp. xx, Oct. 2022.

[9] H. Malmberg, G. Wilckens, and H.-A. Loeliger, "Control-bounded analog-to-digital conversion," *Circuits, Syst. Signal Process.,* vol. 41, no. 3, pp. 1223-1254, Mar. 2022.

[10] H. Malmberg, T. Mettler, T. Burger, F. Feyling, and H.A. Loeliger, "Calibrating control-bounded ADCs," *IEEE International Symposium on Circuits and Systems (ISCAS),* USA, pp. x, 2023.

[11] H. Malmberg, Control-Bounded A/D Conversion Toolbox (cbadc), https://github.com/hammal/cbadc.git, v0.2.2, 2022.